Electronic Supplementary Information
ESI

Network-like arrangement of mixed-valence uranium oxide nanoparticles after glutathione-induced reduction of uranium(VI)

Jerome Kretzschmar,[a]* Toni Haubitz,[ab] René Hübner,[c] Stephan Weiss,[a]
Richard Husar,[a] Vinzenz Brendler[a] and Thorsten Stumpf[a]

[a] Institute of Resource Ecology, Helmholtz-Zentrum Dresden-Rossendorf,
Bautzner Landstr. 400, 01328 Dresden, Germany.

[b] Institute of Chemistry, University Potsdam, Karl-Liebknecht-Str. 24-25,
Building 29, 14476 Potsdam OT Golm, Germany.

[c] Institute of Ion Beam Physics and Materials Research, Helmholtz-Zentrum
Dresden-Rossendorf, Bautzner Landstr. 400, 01328 Dresden, Germany.

*Corresponding author.
E-mail address: j.kretzschmar@hzdr.de

The Electronic Supplementary Information comprises 32 pages, including
1 Scheme, 24 Figures, 4 Tables, and 11 References.

CONTENTS

INSTRUMENTATION

Transmission electron microscopy (TEM)

Samples for TEM measurements were prepared by dropping one drop of the solutions under investigation on a carbon-coated copper grid (400 mesh, S 160, Plano GmbH) and drying it under N_2 atmosphere. Bright-field TEM and high-resolution TEM (HRTEM) images were collected on an image-C_s-corrected Titan 80-300 electron microscope (FEI) operated at 300 kV. Selected-area electron diffraction (SAED) patterns were acquired from a specimen area of 190 nm in diameter. Qualitative atomic number contrast imaging was done by high-angle annular dark-field scanning transmission electron microscopy (HAADF-STEM). Energy-dispersive X-ray spectroscopy (EDXS) was performed with a Li-drifted silicon detector (EDAX).

Ultraviolet-visible(-near infrared) absorption spectroscopy (UV-Vis(-NIR))

UV-Vis spectra were acquired on a J & M Tidas 100 UV-Vis spectrometer in the range between 300 and 800 (1400) nm using a 1 cm quartz cuvette or, where applicable, a 250 cm liquid waveguide capillary cell (LWCC) by World Precision Instruments.

Infrared spectroscopy (IR)

The IR experiments were carried out with a Bruker Vertex 80/v spectrometer, equipped with a mercury cadmium telluride (MCT) detector. Each IR spectrum recorded was an average over 256 scans at a spectral resolution of 4 cm^{-1} using the OPUS software for data acquisition and evaluation.

Nuclear magnetic resonance spectroscopy (NMR)

^{1}H NMR was performed on an Agilent DD2-600 Premium Compact NMR system operating at 14.1 T with a corresponding ^{1}H resonance frequency of 599.82 MHz using a 5 mm oneNMR™ probe. The spectrum of the re-dissolved sample was acquired with suppression of the HDO signal by means of a selective 2 s pre-saturation pulse with offset on the water signal prior to detection. ^{1}H chemical shifts are reported relative to the trimethylsilyl signal of 4,4-dimethyl-4-silapentane-1-sulfonic acid sodium salt (DSS; Sigma-Aldrich, 98%) with δ_H = 0.0 ppm.

Dynamic light scattering (DLS)

Particle size determination in suspensions was performed by dynamic light scattering using a Zetasizer Nano ZS (Malvern Instruments) device.

EXPERIMENTAL DETAILS

All preparation steps were performed with safety precautions according to the radioactivity of natural uranium (U-nat.).

Reaction samples were prepared under nitrogen atmosphere by mixture of appropriate volumes of a U(VI) stock solution made of UO_3 by dissolution in 0.5 M DCl (Deutero, 37% in D_2O with 99% D) and D_2O (Deutero, 99.98% D) solutions of glutathione (GSH; Roth, $\geq 98\%$) in order to obtain 3 ml solutions with 6.67 mM in GSH and U(VI) concentrations in the range of 0.33 mM through 6.67 mM. Throughout this series also samples at varying pD values (2–10) were investigated with pD adjustment achieved by addition of diluted D_2O solutions of DCl and NaOD (Deutero, 40% in D_2O with 99% D) with pD = pH + 0.4, and probed with NMR spectroscopy.

Depending on the several analyses and spectroscopic methods, the samples were further processed according to Scheme S1.

For TEM aliquots of both a freshly prepared non-centrifuged yellow suspension of initially 6.67 mM GSH and 3.33 mM pD 7 as well as a decanted supernatant after centrifugation (1 h at $5500 \times g$) of a former analogue after aging for 2 months, were used.

The yellow precipitate was analysed after centrifugation (1 h at $5500 \times g$), decanting the supernatant (for aging) and three times iteratively re-dispersed with 1 M NaCl solution and centrifuged prior to lyophilisation, discarding the supernatants of these washing steps. The dry powder was used as obtained for IR spectroscopy (KBr pellet). For UV-Vis spectroscopy ≈ 5 mg were dissolved in 5 M $HClO_4$ (Sigma-Aldrich, 99.99%) and for ^{1}H NMR analysis ≈ 10 mg were dissolved in 1 ml 0.5 M DCl D_2O solution.

U(VI) STOCK SOLUTION

$UO_3 + 0.5\ M\ DCl \rightarrow UO_2^{2+}$

GSH STOCK SOLUTION

GSH dissolved in D_2O

$UO_2^{2+}{}_{(aq)} + GSH_{(aq)}$

PS 1
sample series

- GSH 6.67 mM
- pD variation (adjustment with NaOD/DCl)
- U content variation [0.33–13.33 mM]

TEM

PS 2
centrifugation

supernatant

pellet

3× iterative washing
with 1 M NaCl and
centrifugation;
supernatants
discarded

NMR

PS 3
lyophilization

PS 4
ageing

PS 4
ageing

addition of 1 mL MilliQ-H_2O
and re-dispersion by
ultrasonication

dissolution in 1–5 M $HClO_4$

DLS

TEM

UV-Vis

extraction
with 1 M
K_2CO_3

DLS

PS 5
centrifugation

NMR

dissolution in
0.5 M DCl

KBr
pellet

supernatant
discarded

UV-Vis
LWCC

dissolution in
5 M $HClO_4$

contd
ageing

IR

dissolution in
1 M $HClO_4$

UV-Vis
(-NIR)

dissolution in
11 M $HClO_4$ and 0.2 µm filtration

Scheme S1. Preparation scheme showing the processing steps (PS) and analyses, as well as photographs of the samples at different stages of processing.

Brief characterization of U(VI)–GSH precipitate
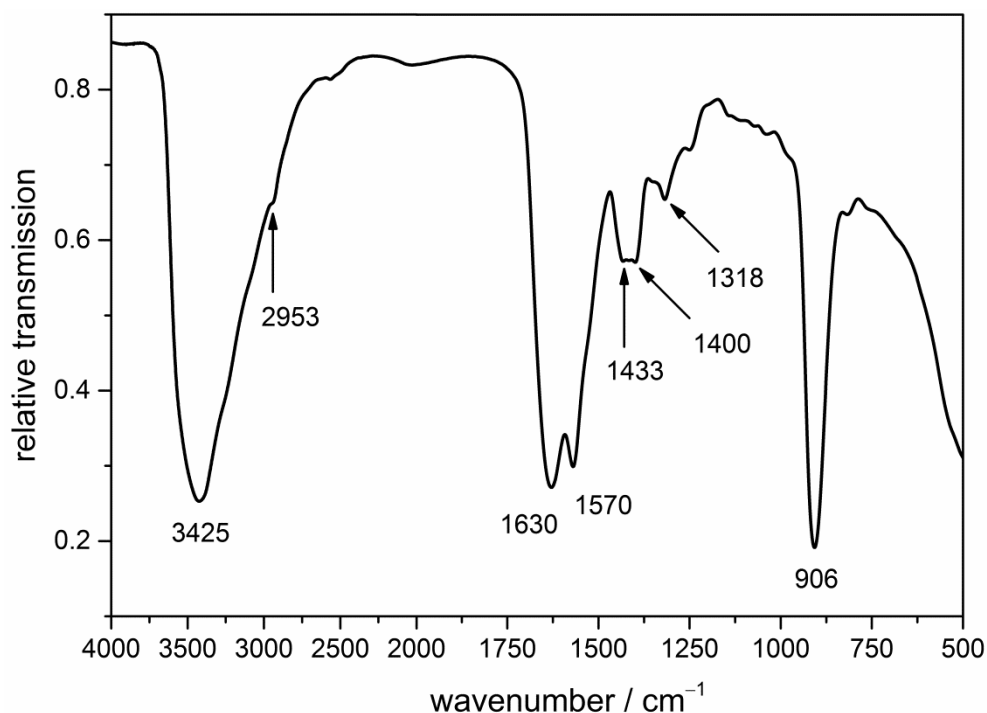
Fig. S1. IR spectrum (KBr pellet) of the lyophilized pellet obtained from solutions of GSH and U(VI) at molar ratio of 5 : 1 at pD 5.

Table S1. Band assignment and interpretation of the IR spectrum shown in Fig. S1.

wavenumber / cm^{-1}	intensity	assignment	structure/fragment
3425	vs, b	$\nu(OH) + \nu(NH)$	water/OH + amide (GSH)
2953	w	$\nu(CH, sp^3)$	aliphatic CH_2 (GSH)
1630 – 1570	vs	$\nu_{as}(COO)$ (+ CONH)	carboxylate (GSH) + amide I/II
1433 – 1400	m	$\nu_s(COO)$	carboxylate (GSH)
1318	w	$\nu(C–N)$	GSH (glu ammonium)
906	vs	$\nu_{as}(O=U=O)$	UO_2^{2+}

vs: very strong, b: broad, w: weak, m: medium; ν: stretching, s: symmetric, as: antisymmetric

Since characteristic vibrational bands of uranium hydrolysis species occur at 923 (pH 5), 1525 and 1460 cm^{-1}, the pure (binary) uranyl hydroxo species can be excluded. Furthermore, due to the absence of vibrational bands at 1365 and 893 cm^{-1} also uranyl (hydroxo)carbonate species can be excluded.[1]
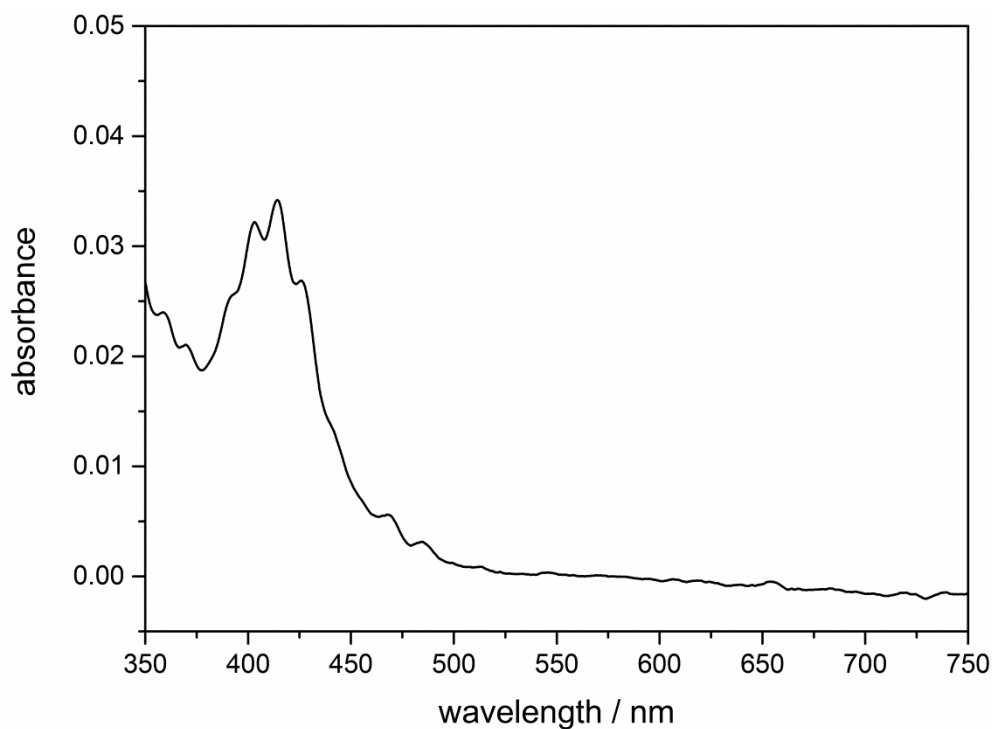
Fig. S2. UV-Vis spectrum (d = 1 cm) of the lyophilized pellet obtained from D_2O solutions of GSH and U(VI) at a molar ratio of 5 : 1 at pD 5 after dissolution in 5 M $HClO_4$.

Table S2. UV-Vis absorption maxima according to Fig. S2. Values in parentheses represent absorption maxima assigned to free U(VI) according to Ref. 2.

observed (literature) absorption maxima / nm
369.5 (369.9)
391.0 (391.6)
402.9 (402.7)
414.2 (414.5)
425.9 (427.0)
468.1 (468.8)
484.6 (484.6)
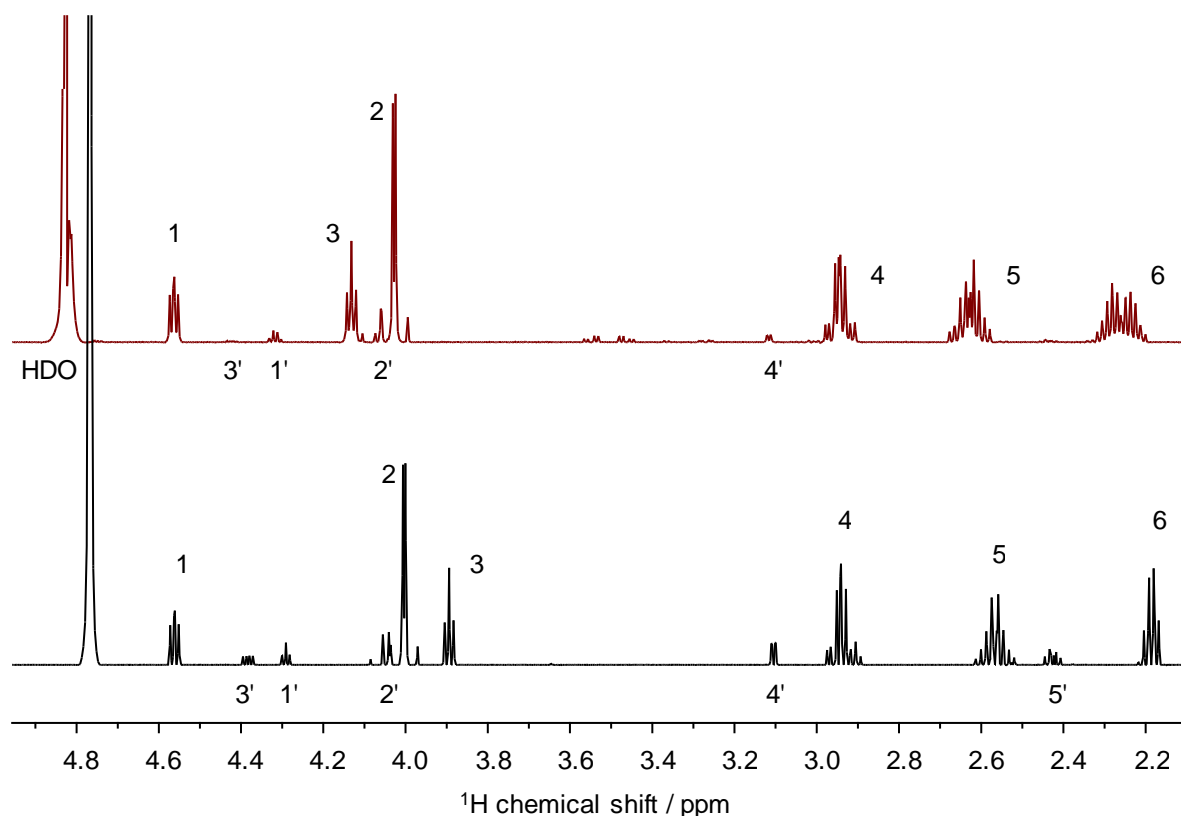
Fig. S3. ^{1}H NMR spectra (600 MHz) of ≈ 10 mg of the lyophilized U(VI)–GSH pellet after dissolution in 1 ml 0.5 M DCl (top) and GSH in D_2O at pD 2 (bottom). Signals of GSH: **1** cys α, **2** gly α, **3** glu α, **4** cys β, **5** glu γ, **6** glu β. Note: 15% decomposition of GSH into cysteinyl-glycine (**1'** cys α, **2'** gly α, **4'** cys α) and glutamate (**3'** glu α; **5'** glu γ, and glu β overlapping with **6**) owing to the acidic conditions; chemical shift differences between spectra due to different pD.

IR (Fig. S1 and Table S1) and UV-Vis (Fig. S2 and Table S2) spectroscopy revealed uranium in its +VI oxidation state as indicated by the antisymmetric stretching, ν_3(O=U=O) appearing at 906 cm^{-1}, and characteristic absorption maxima, respectively. The bathochromic shift of ν_3 (as compared to 962 cm^{-1} for the free UO_2^{2+}) and the GSH content found by NMR spectroscopy after re-dissolution of the lyophilized precipitate in 0.5 M DCl (Fig. S3) revealed the precipitate to consist of U(VI)–GSH complexes, likely being ternary U(VI) hydroxo GSH complexes. The obtained yellow precipitate containing GSH unbound to U(VI) can be ruled out since GSH itself is very well soluble and co-precipitation is hence very unlikely, but even if so, it had been removed by the washing steps (see Scheme S1).
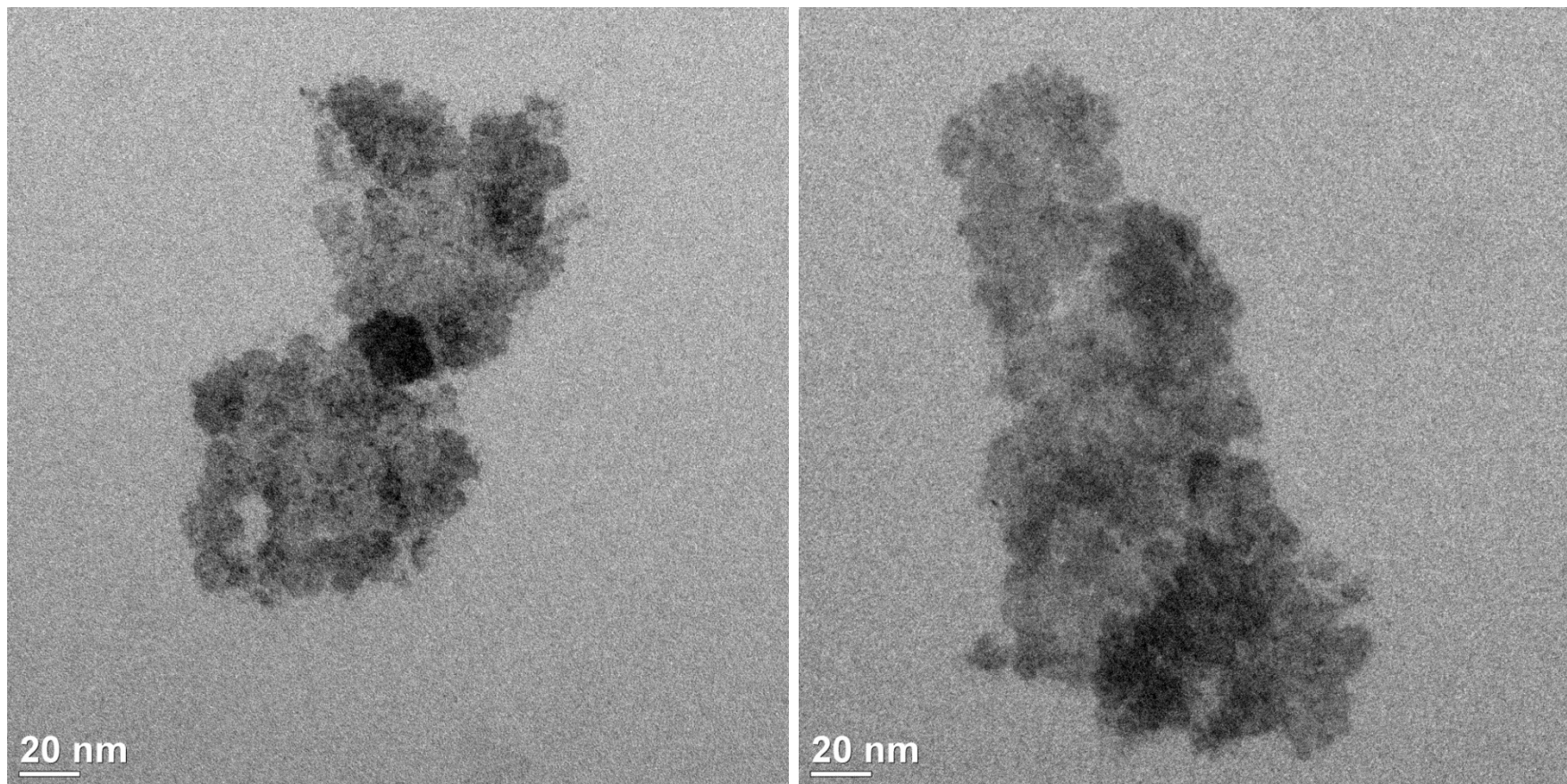
Fig. S4. Bright-field TEM micrographs of two representative specimen areas obtained from the dried precipitate of the non-centrifuged sample suspension (between PS 1 and PS 2 in Scheme S1) of initial 6.67 mM GSH and 3.33 mM U(VI) at pD 7.
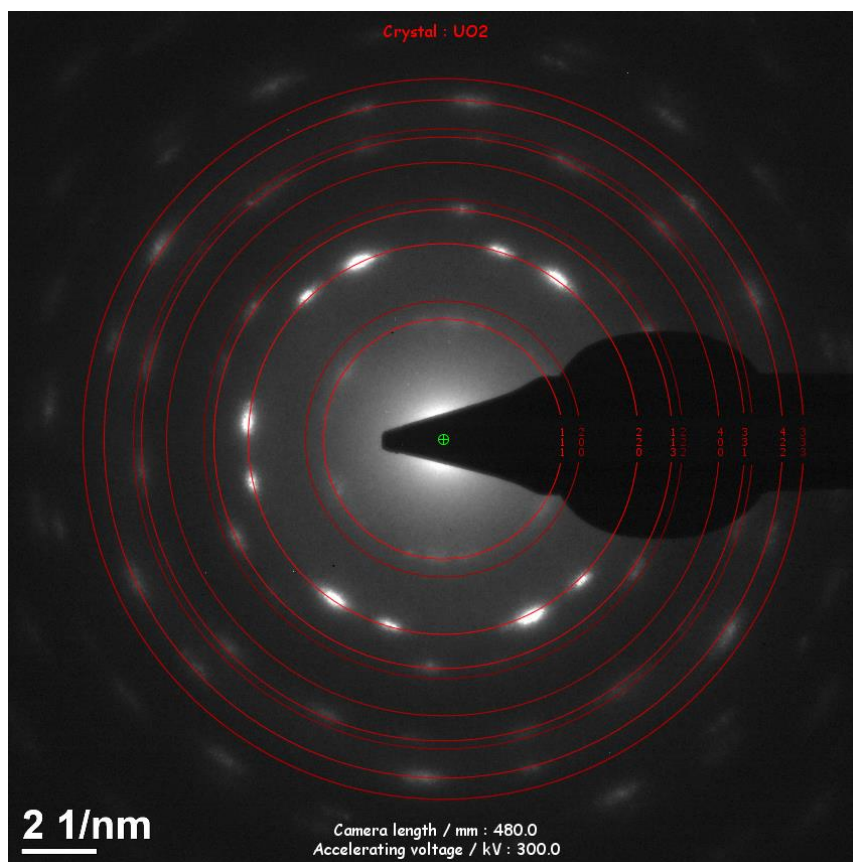
Fig. S5. SAED pattern obtained from the precipitate shown in the right image of Fig. S4. The red rings belong to the simulated diffraction pattern based on fluorite-type UO_2 (ICSD card 24224) indicating that the precipitate is composed of crystalline $UO_{2(+x)}$.
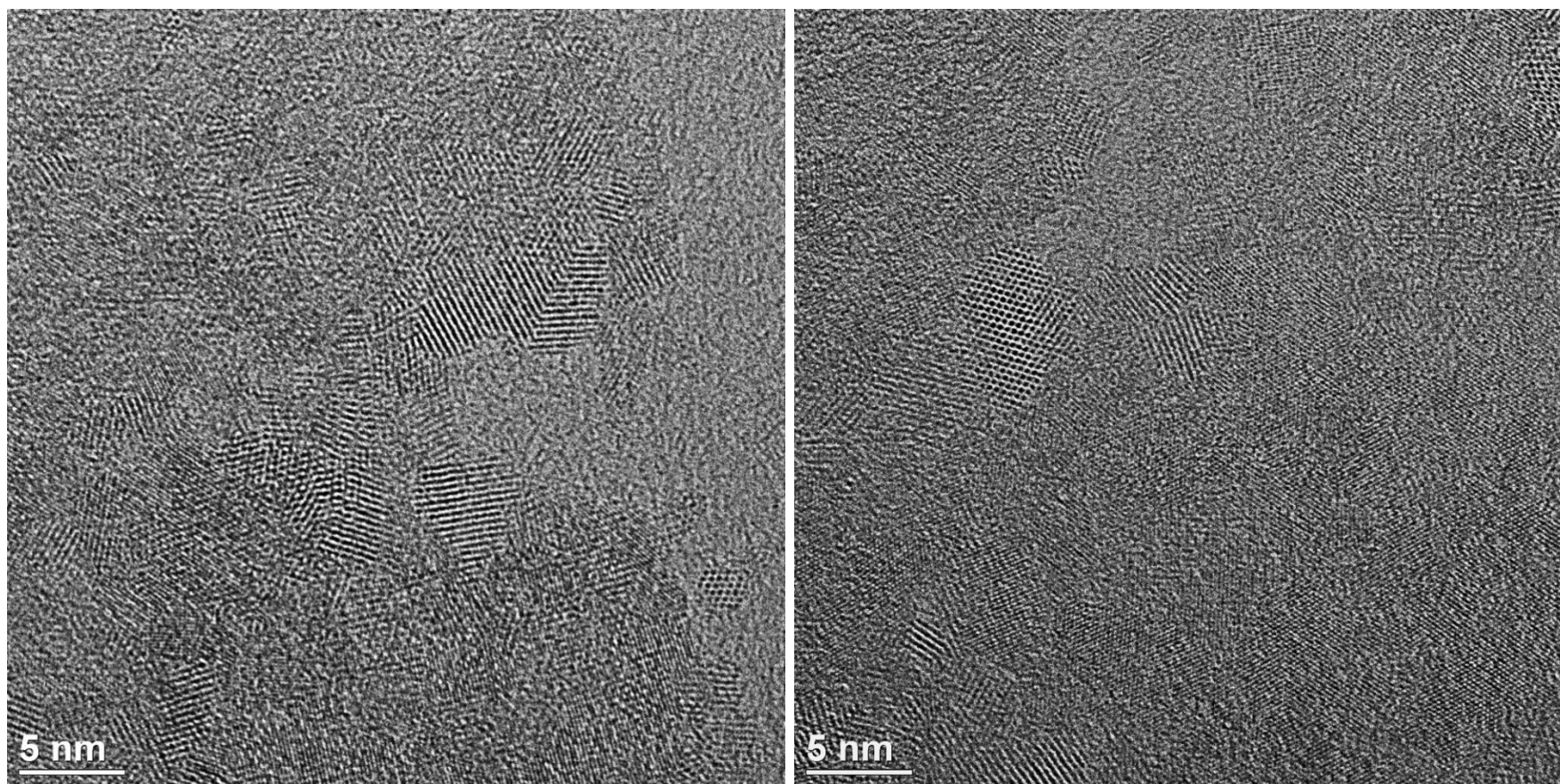
Fig. S6. HRTEM micrographs of two different specimen positions obtained from the precipitate shown in the right image of Fig. S4.
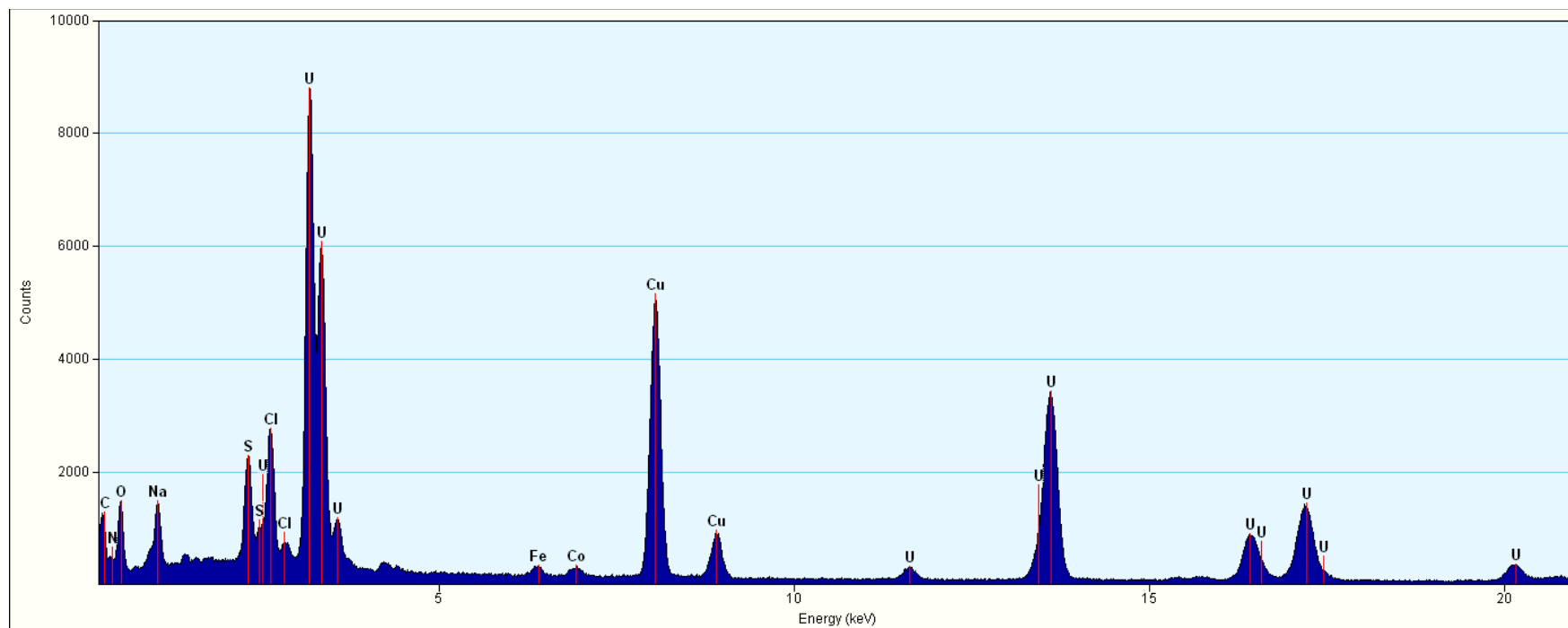
Fig. S7. Energy-dispersive X-ray (EDX) spectrum obtained with a condensed electron beam in TEM mode of the dried precipitate obtained from the non-centrifuged sample suspension (between PS 1 and PS 2 in Scheme S1). The C and Cu signals are associated with the carbon-coated copper grid used for the TEM measurement. Fe and Co are fluorescence signals from the pole piece of the microscope objective lens.

The N and S signals are unambiguously attributed to GSH, whereas Na and Cl are residuals from pD adjustment (DCl, NaOD). The former signals show that the freshly prepared (6.67 mM GSH / 3.33 mM U(VI) / pD 7) sample contains both the (expected) U(VI)–GSH complex and, interestingly, within minutes after preparation, reduced uranium appearing as nc-$UO_{2(+x)}$ (Figs. S5 and S6).

Characterization of network-like arranged UO_{2+x} nanocrystals (aged supernatant)
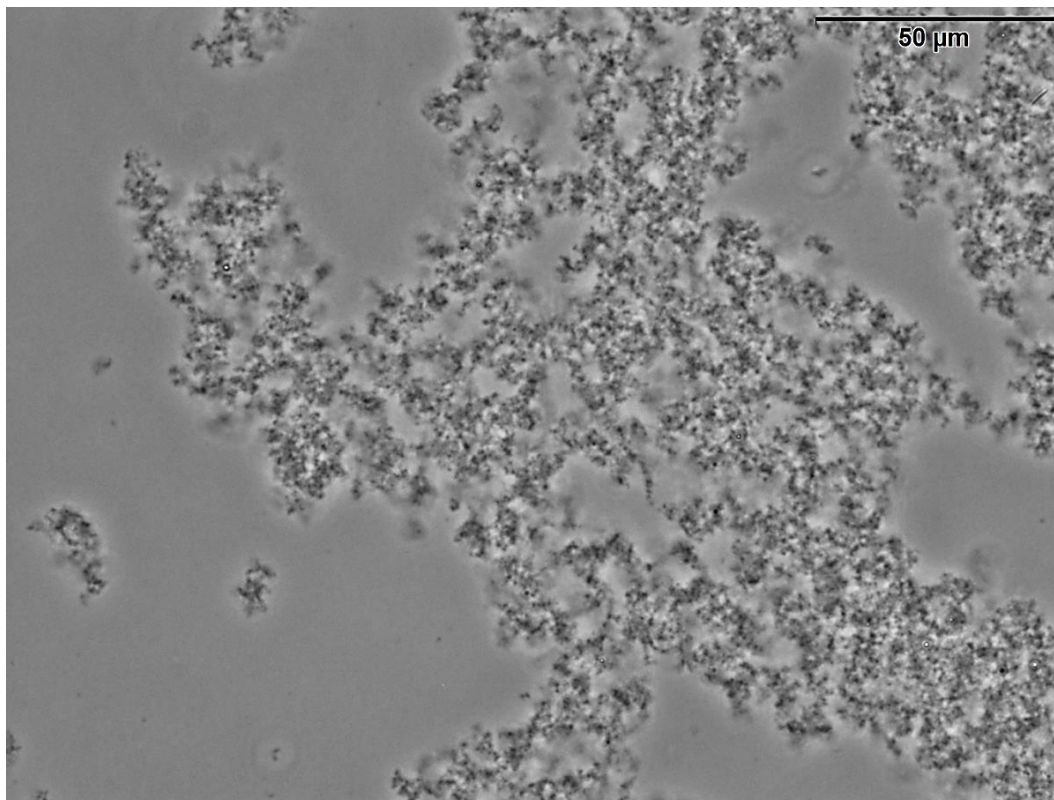
Fig. S8. Light microscope image of the aged supernatant (according to the solution between PS 4 and PS 5 in Scheme S1).
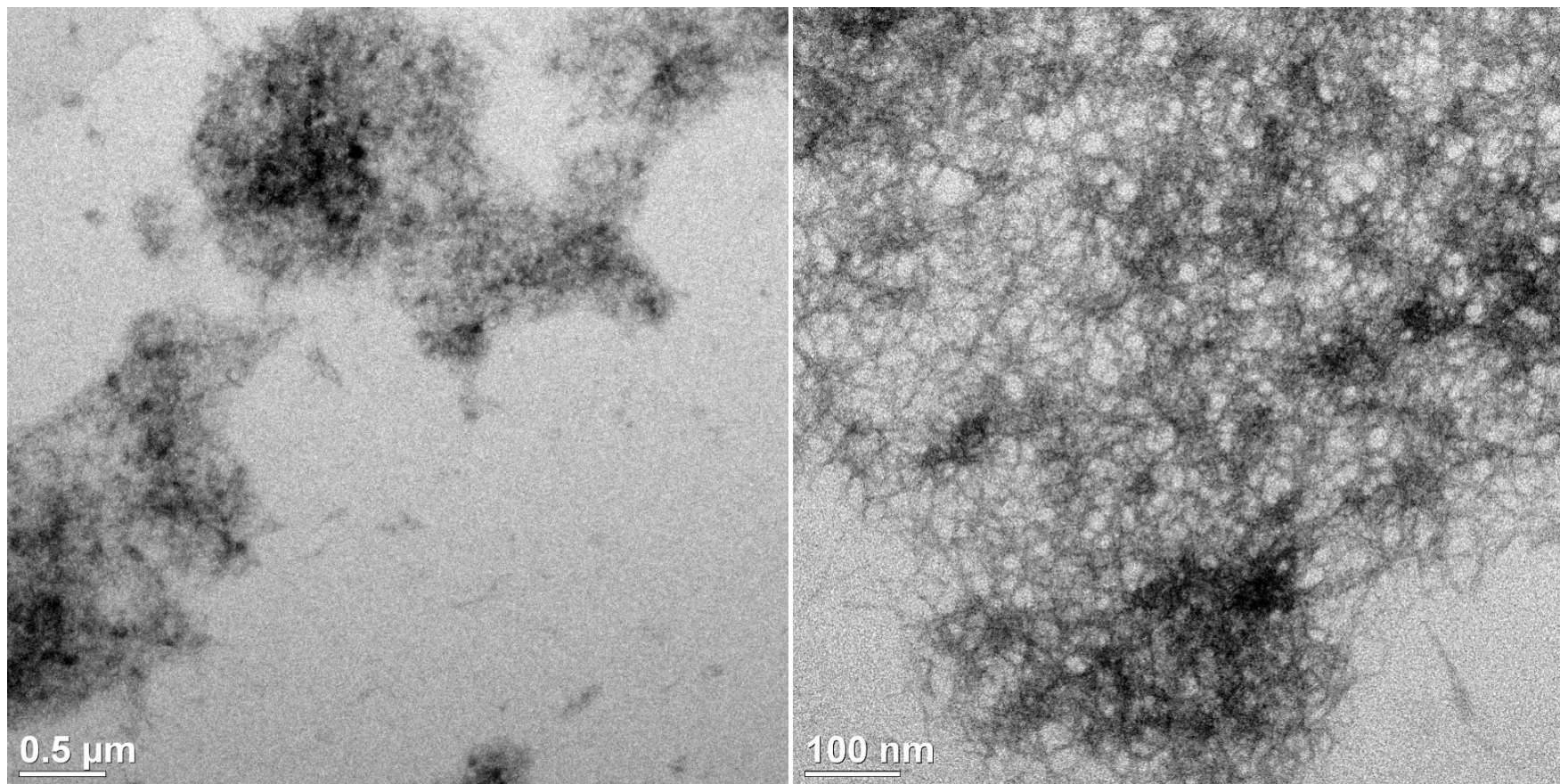
Fig. S9. Bright-field TEM images at different magnifications (*cf.* Fig. 2) of the dried precipitate obtained from the aged supernatant (according to the solution between PS 4 and PS 5 in Scheme S1) of the sample of initial 6.67 mM GSH and 3.33 mM U(VI) at pD7.
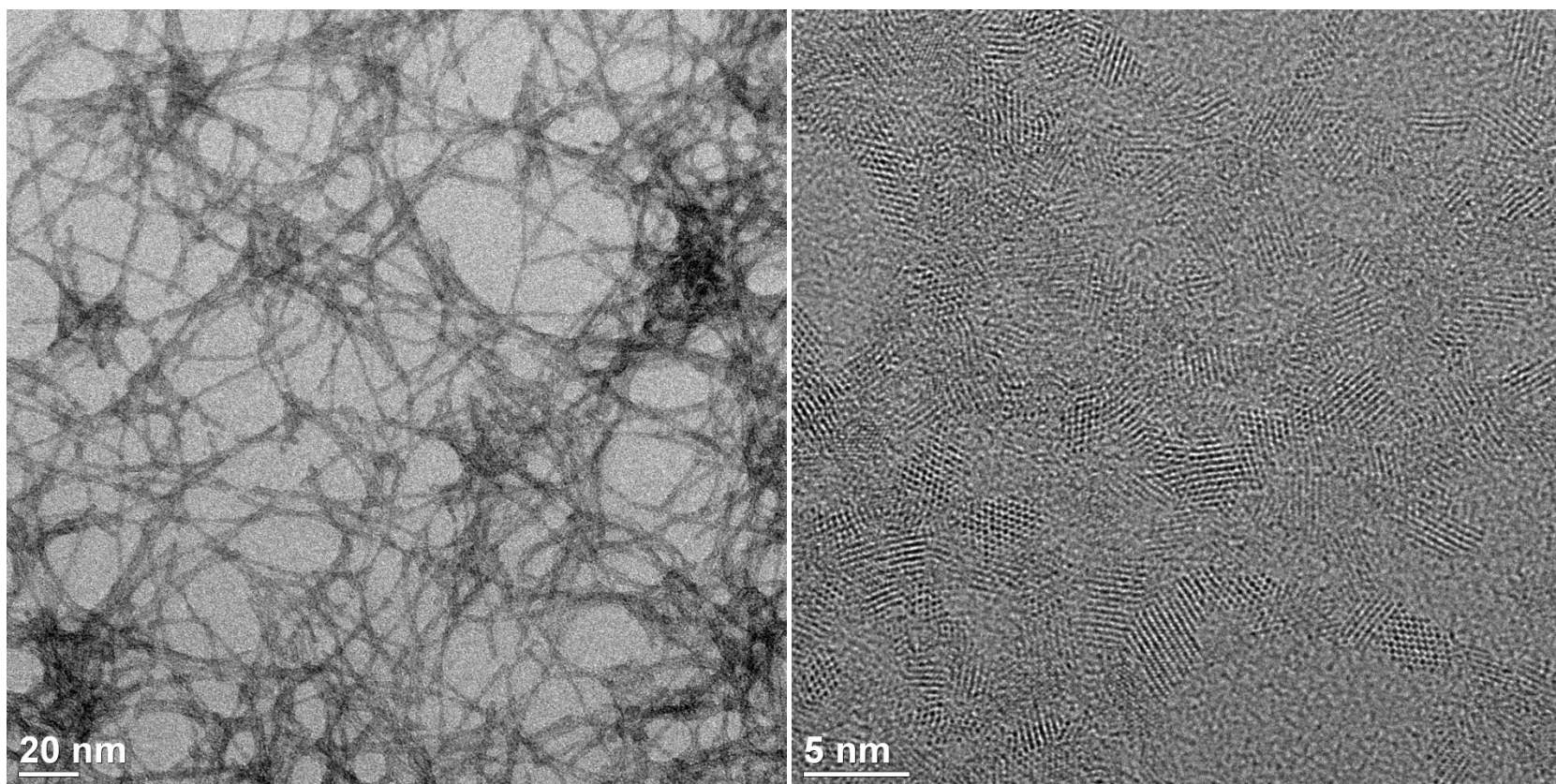
Fig. S10. TEM micrographs at different magnifications (*cf.* Fig. 2) of the dried precipitate obtained from the aged supernatant (according to the solution between PS 4 and PS 5 in Scheme S1) of the sample of initial 6.67 mM GSH and 3.33 mM U(VI) at pD 7.
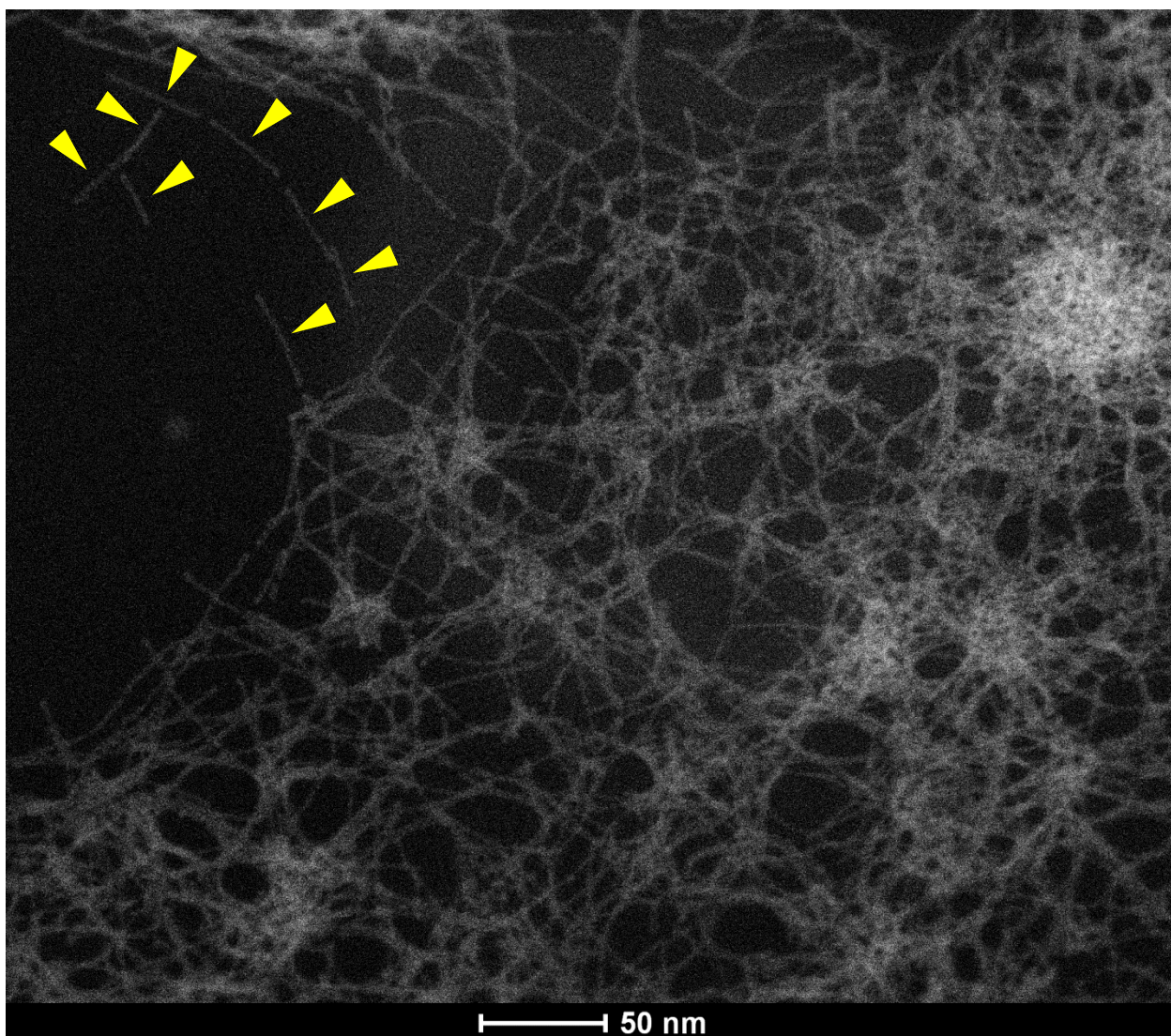
Fig. S11. HAADF-STEM micrograph of the dried precipitate obtained from the aged supernatant (according to the solution between PS 4 and PS 5 in Scheme S1) of the sample of initial 6.67 mM GSH and 3.33 mM U(VI) at pD 7, with yellow spearheads indicating some chain-like building blocks.

This STEM micrograph reveals some connected nanocrystals – the initial building blocks – that form ~ 20–40 nm sized chain-like units (indicated by yellow spearheads) that can be considered as higher building blocks that further associate either "end-on", appearing as extended chains, or "side-on" causing branching.
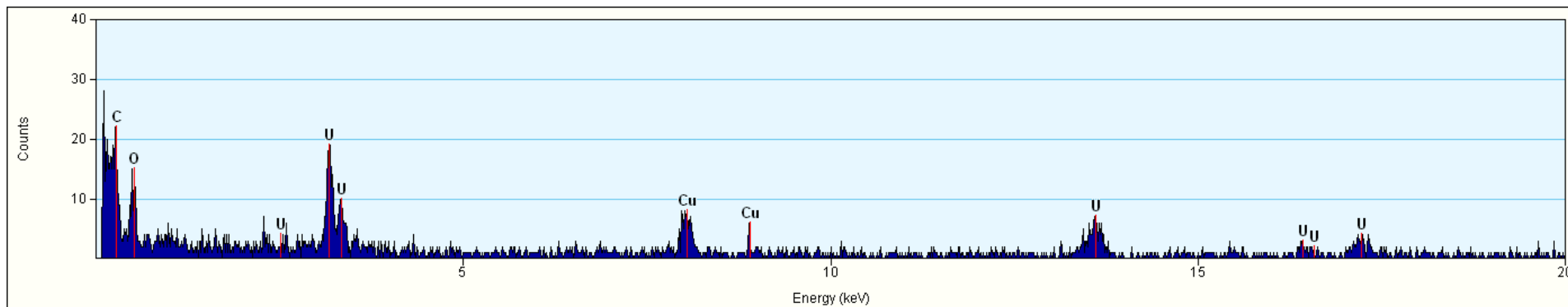
Fig. S12. Energy-dispersive X-ray (EDX) spectrum (top) obtained in HAADF-STEM mode of a representative sample region (right) of the dried precipitate obtained from the non-centrifuged sample suspension (between PS 4 and PS 5 in Scheme S1). The C and Cu signals are associated with the carbon-coated copper grid used for the STEM measurement.

As compared to the EDX spectrum of the U(VI)–GSH precipitate (Fig. S7), the material was not as dense due to both the remarkable spacing in the network-like morphology and the lower overall loading on the TEM grid (since prepared from the much less GSH- and U-containing (aged) supernatant). Supporting the composition of the nanoparticles, the only significant material-based signals are associated with U and O.
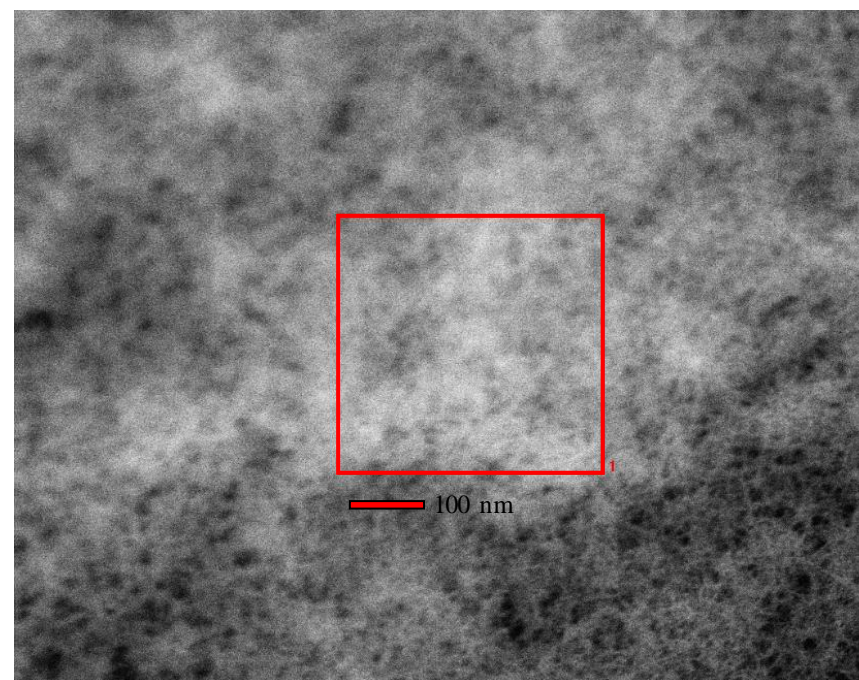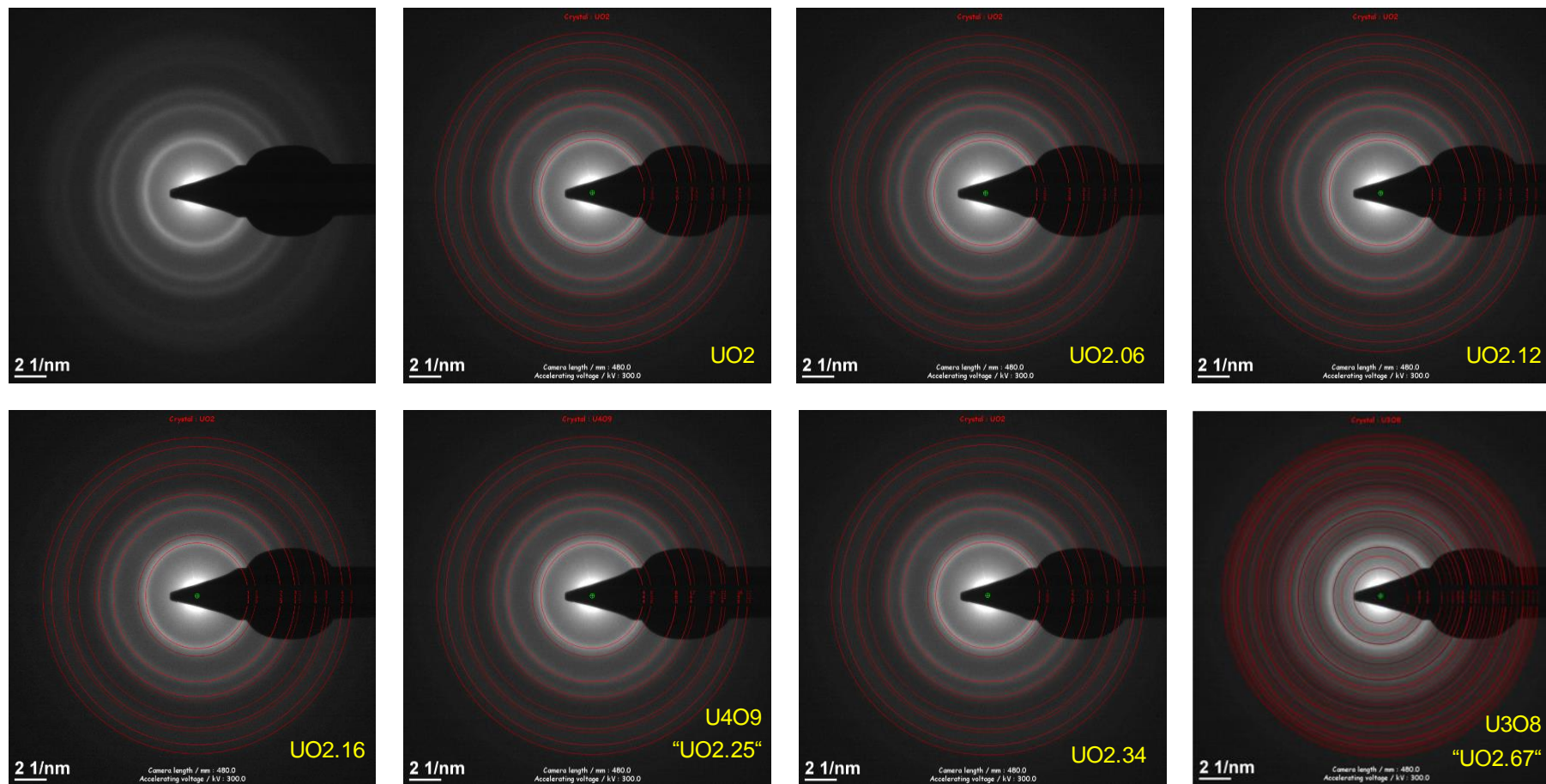
Fig. S13. Experimentally obtained SAED pattern (upper left) of the aged pale brownish supernatant of the initial 6.67 mM GSH 3.33 mM U(VI) pD 7 sample and trial-and-error matching attempts with simulated diffraction patterns (red rings) for different UO_x structures based on reference data: ICSD 24224 (UO_2); ICSD 108858 ($UO_{2.06}$); ICSD 1426 ($UO_{2.12}$); ICSD 95295 ($UO_{2.16}$); ICSD 15439 (U_4O_9); ICSD 29137 ($UO_{2.34}$); ICSD 246854 (U_3O_8).
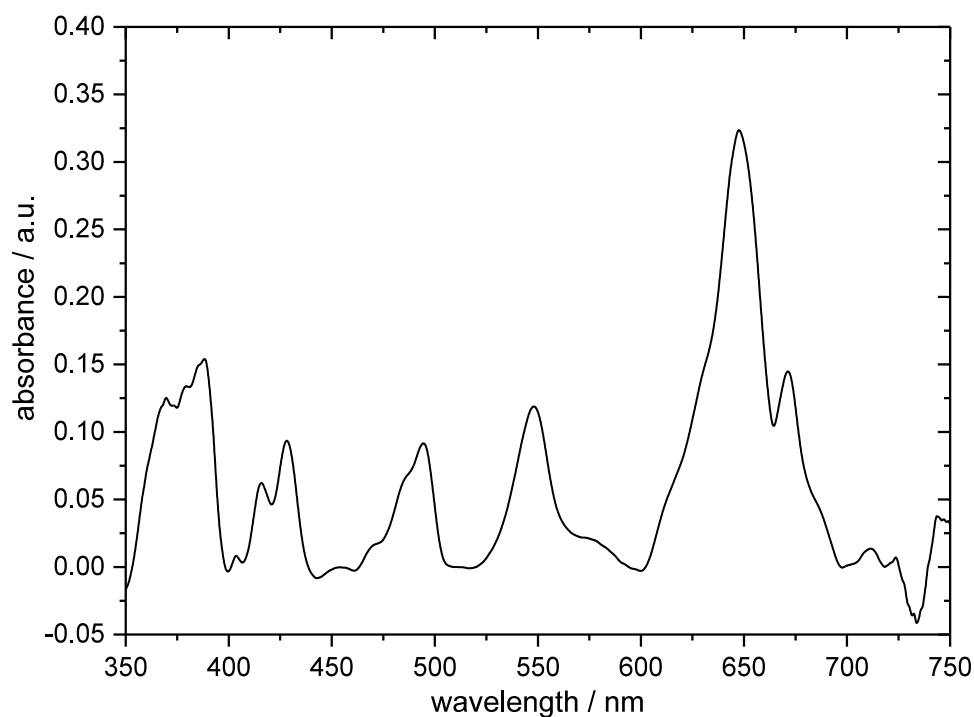
Fig. S14. UV-Vis spectrum of the brownish pellet obtained from aged and centrifuged supernatant of the sample of initial 6.67 mM GSH and 3.33 mM U(VI) at pD 7, according to Scheme S1 (PS 5), after dissolution in 5 M HClO$_4$. Note that this spectrum was obtained using a 250 cm liquid waveguide capillary cell (LWCC, d = 250 cm); band positions summarized in Table S3.

Table S3. UV-Vis absorption maxima according to Fig. S14.

observed (literature) absorption maxima / nm	assignment
369.5 (369.9)[a]	UO$_2^{2+}$
393.0 (391.6)[a]	UO$_2^{2+}$
408.6 (407.7)[a]	UO$_2^{2+}$
414.9 (414.5)[a]	UO$_2^{2+}$
428.3 (427.0)[a] / (429.4)[b]	UO$_2^{2+}$ / U^{4+}
468.1 (468.8)[a]	UO$_2^{2+}$
485.2 (484.6)[a] / (485.9)[b]	UO$_2^{2+}$ / U^{4+}
495.1 (495.3)[b]	U^{4+}
548.0 (549.5)[b]	U^{4+}
647.5 (648.5)[b]	U^{4+}
671.0 (671.6)[b]	U^{4+}

[a] Ref. 2; [b] Ref. 3
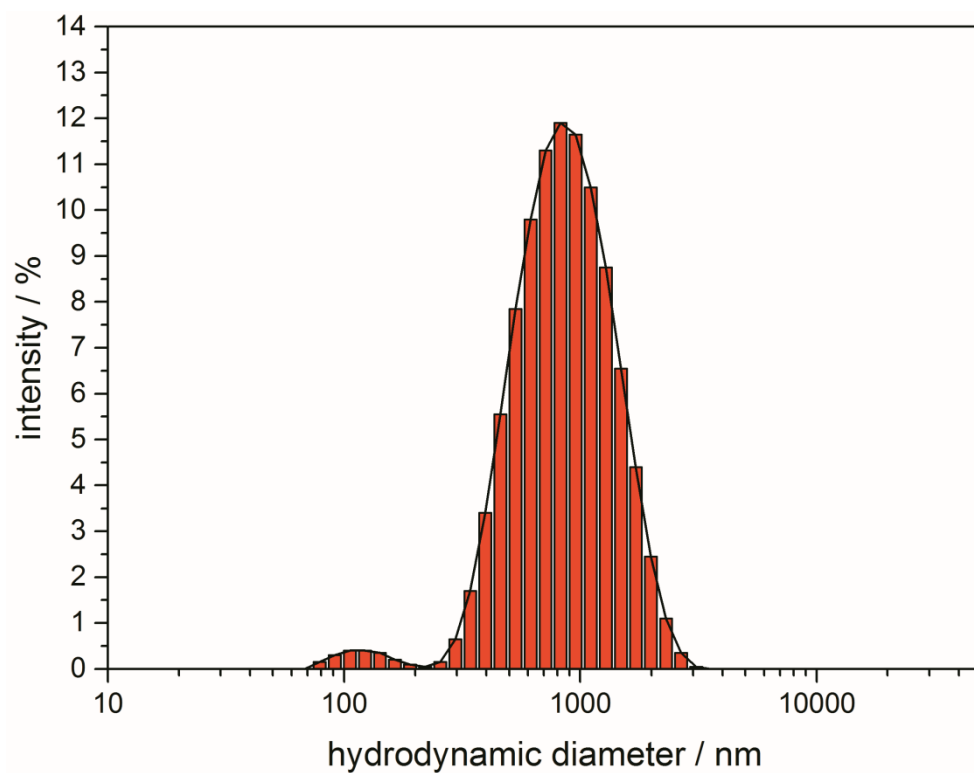
Fig. S15. Particle size distribution of the non-centrifuged, aged pale brownish supernatant of the sample of initial 6.67 mM GSH and 3.33 mM U(VI) at pD 8, (according to the solution between PS 4 and PS 5 in Scheme S1), determined by DLS. Note that the quantity of the smaller particles is potentially underestimated.
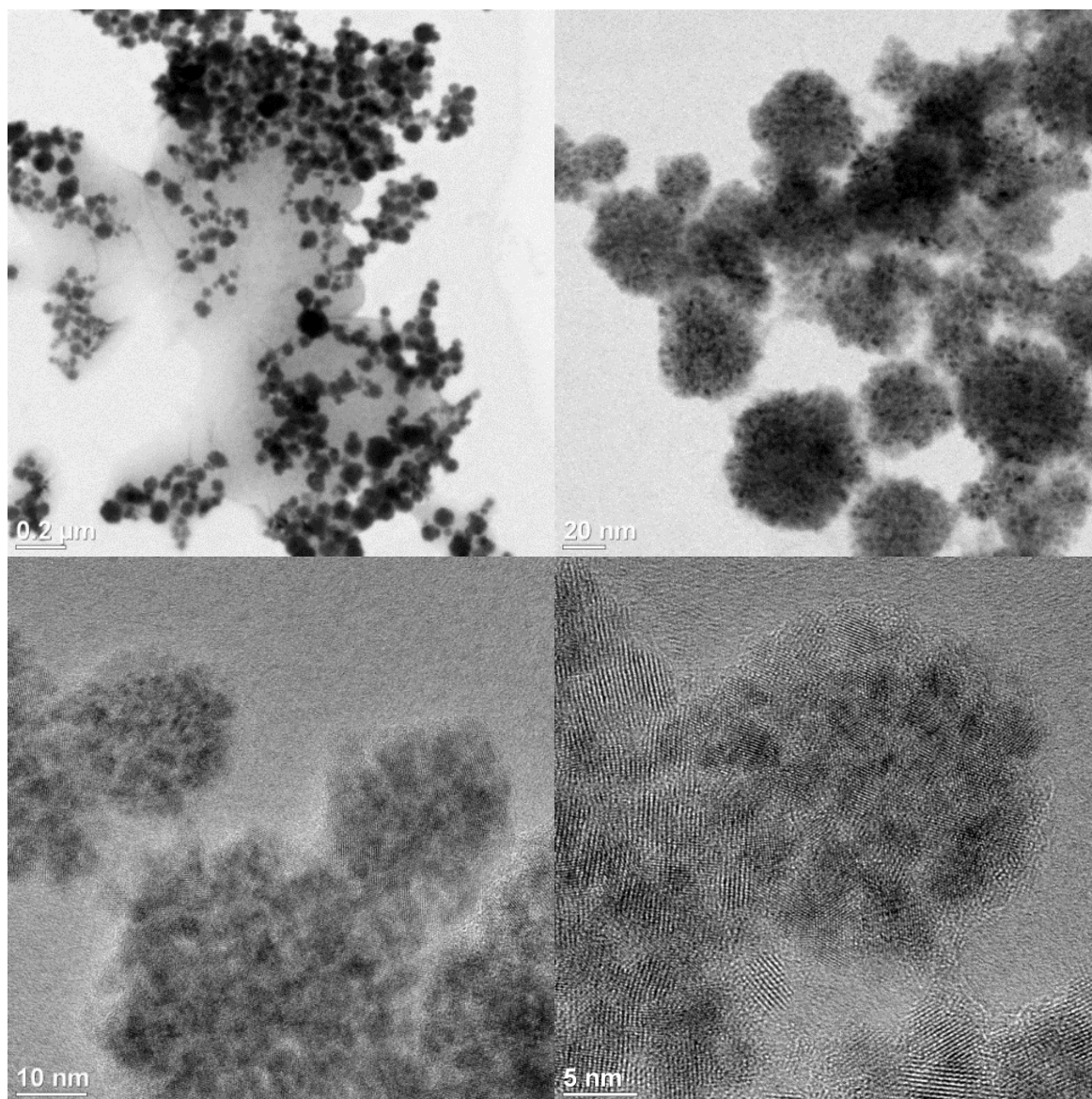
Fig. S16. TEM micrographs of the dark grey precipitate obtained *after light-irradiation* of a 6.67 mM GSH and 3.33 mM U(VI) pD 2.25 sample at different magnifications. Note the NaCl matrix appearing light grey in the upper left image is due to TEM specimen preparation by solvent evaporation.

Consideration of the redox reaction and its mechanistic implications (aged wet paste pellet)
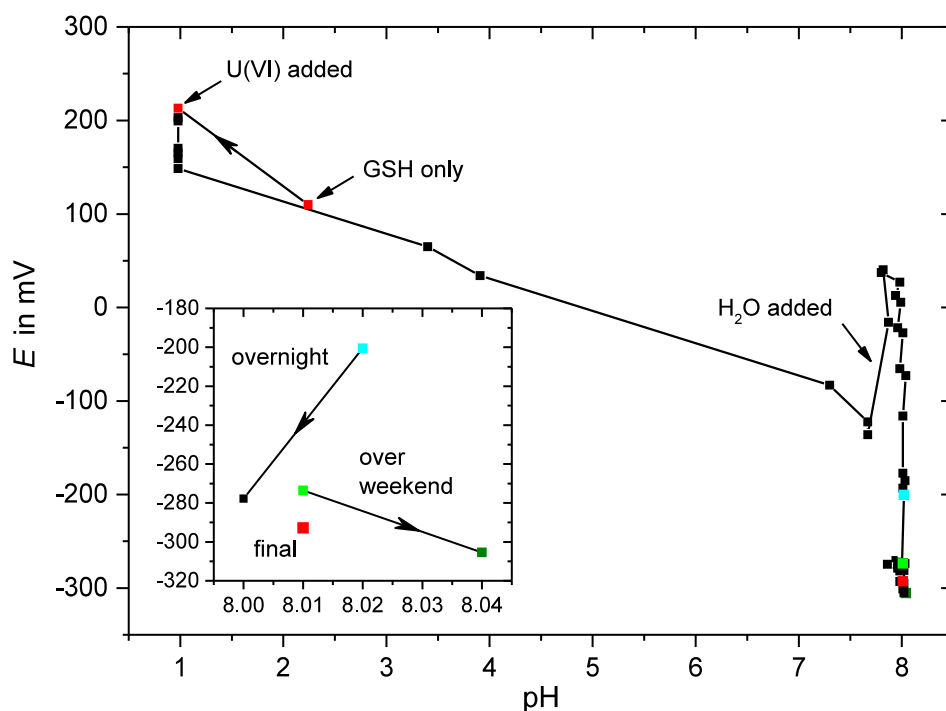
Fig. S17. Redox potential E during pH adjustment of a 10 mM GSH and 5 mM U(VI) sample with continuous stirring. Data points correspond to pH/E values recorded after some equilibration.

As shown in Fig. S17, initially, that is for low pH which is equal to high [H$^+$], the redox potential is positive for both the GSH-only solution ($E° = +180$ mV)[4] and after admixture of U(VI) solution (pH < 1), see correspondingly indicated data points. Upon successive addition of NaOH, primarily the Gly COOH (pK_a 3.20 ± 0.03) is titrated and U(VI) changes its speciation from free uranyl ion to (polynuclear) hydroxo species, with concomitant formation of ternary GSH hydroxo U(VI) complexes. The large step, *i.e.* pH 3.91→7.30, is due to totally titrated Gly COOH, thus used up buffering capacity. As of circumneutral conditions, E becomes negative. Addition of water (for total volume adjustment; as indicated) temporarily increases E due to dilution effects, but around the designated final pH 8 E becomes remarkably negative, since GSH's SH group (pK_a 9.01 ± 0.07) starts to ionise and, therefore, develops its full reduction potential. In order to achieve pH stability, the solution was allowed to stand overnight and the next day pH has changed only little, whereas E dropped considerably (see insert; note the scaling). After some further adjustment throughout the day, the solution was then allowed to equilibrate over the weekend, showing pH stability but even more negative E value. With a finally recorded pH/E of 8.01/−293 mV the solution was allowed to age.

Note that the pK_a values were (re-)determined as part of this work by means of NMR titration and corresponding sigmoidal fits of the chemical shift *vs.* pD plots, with inflection points representing pK_a (data not shown).

$$GS\text{–}H + H\text{–}SG \longrightarrow GS\text{–}SG + 2\,H^+ + 2\,e^- \tag{1}$$

$$UO_2^{2+} + 2\,e^- + 4\,H^+ \longrightarrow U^{4+} + 2\,H_2O \tag{2}$$

$$UO_2^{2+} + e^- \longrightarrow UO_2^+ \tag{3}$$

$$2\,UO_2^+ + 4\,H^+ \longrightarrow U^{4+} + UO_2^{2+} + 2\,H_2O \tag{4}$$
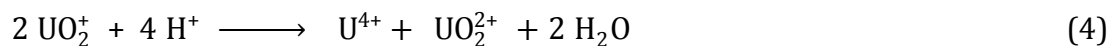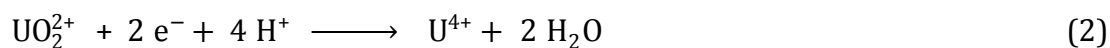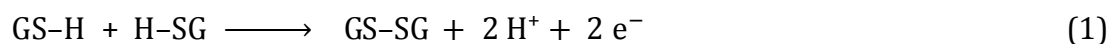
Already the (formal) half-cell reaction equations disclose that the pH dependencies of electron release from GSH, Eqn. (1), and acceptance by UO_2^{2+} to form U^{4+}, Eqn. (2), work in opposite directions, whereupon ΔG becomes progressively less negative with increasing pH and, therefore, the reaction unlikely to take place. Eqn. (1) nicely reveals that GSH becomes more reductive with increasing pH, whereas the formation of U(V) is independent of pH. The subsequent disproportionation of U(V) to U(IV) and U(VI), Eqn. (4), is irreversible and strongly pH dependent, *i.e.* favoured with increasing acidity, explaining the better observability of U(V) at higher pH values (*vide infra*).

Although for alkaline media the pH conditions are well suited for the redox reaction to yield uranium in its +V state, there must be some other reasons preventing the reaction for high pH values. Particularly the reaction shown in Eqn. (5) is in very agreement with the finding that as of pD 10 the redox reaction does not happen any longer owing to (heterolytic) deprotonation of the thiol group (according to its pK_a of 9.0). Obviously, in order to yield a hydrogen atom ($H^+ + e^-$) as the effective reduction equivalent, the S–H bond requires homolytic cleavage (Eqn. (6)), being in accordance with molecular dynamics[5] that the S–H group behaves as a hydrophobic group and is not immediately solvated. A concerted two-electron transfer, *i.e.*, upon disulphide formation (Eqn. (1)) electrons are released in pairs that facilitate direct U(VI)/U(IV) reaction, requiring a transition state including the UO_2^{2+} and two GSH simultaneously acting together, is considered to be very unlikely. Instead, it is more probable that GSH reacts consecutively upon formation of both a hydrogen atom and a thiyl radical, Eqn. (6), the latter too short-lived to be observable by NMR, and supposed to relax by self-terminating (upon electron pairing) second-order reactions finally yielding GSSG, Eqn. (7).

$$G\text{–}S\text{–}H \longrightarrow G\text{–}S^- + H^+ \tag{5}$$

$$G\text{–}S\text{–}H \longrightarrow G\text{–}S^\bullet + H^\bullet \quad (H^\bullet = H^+ + e^-) \tag{6}$$

$$G\text{–}S^\bullet + {}^\bullet S\text{–}G \longrightarrow GS\text{–}SG \tag{7}$$
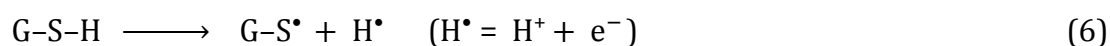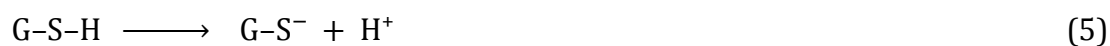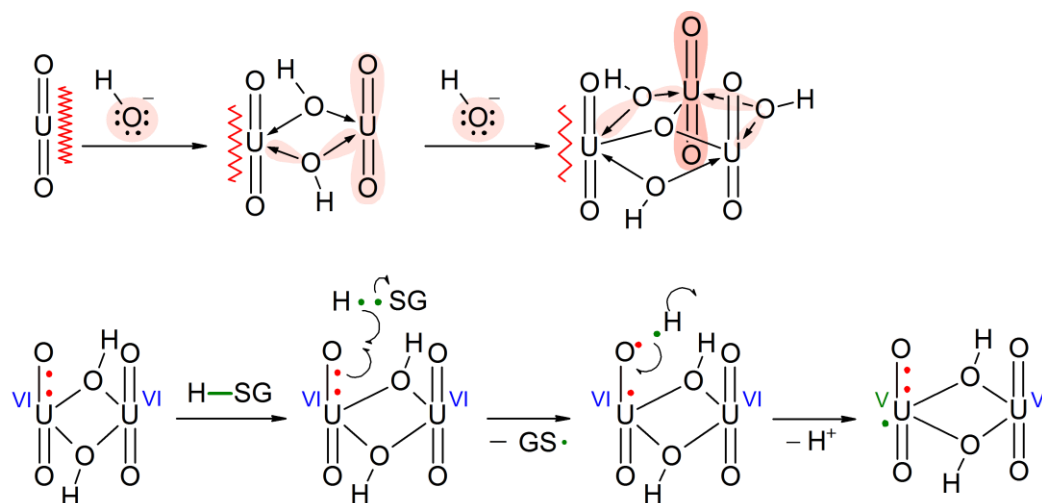
Fig. S18. Illustration of increase in electron density (pale red background) of U–O$_{ax}$ bond and its decrease in bond force constant (symbolised by spring) upon hydroxo ligand coordination as well as formation of polynuclear species (top); hypothetic mechanism of hydrogen-atom-transfer based reduction of U(VI) to U(V) by GSH *via* U–O$_{ax}$ (bottom).

Due to the large positive charge at the uranium centre, upon binding of ligands, *i.e.* Lewis bases, on the one hand, the O=U=O entity withdraws electron density and, hence, exhibits decreasing Lewis acidity in agreement with red-shift of transitions in UV-Vis absorption spectra (decrease of the HOMO–LUMO gap) and weakening of the U–O$_{ax}$ bond force constant and the concomitant decrease in O=U=O vibration frequencies as observed in vibrational spectroscopies. This is well established and nicely seen for, *e.g.*, carboxylate, carbonato or hydroxo ligands. Accordingly, on the other hand the ligands' Lewis basicity decreases. Therefore, polynuclear species bearing these structural motifs are supposed to be better suited than the free uranyl ion to be reduced to U(V). Hypothetic mechanism of hydrogen atom transfer from GSH according to Eqn. (6) for the reduction of U(VI) to U(V) *via yl*-oxygen is sketched in Fig. S18.

U(V) shows a significantly reduced Lewis acidity owing to the decreased cation charge since the "additional 5f electron in UO$_2^+$ occupies a nonbonding 5f_δ orbital and induces a weakening of both axial and equatorial bonds as reflected by the increase of 0.10 and 0.09 Å in the U–O$_{yl}$ and U–water bond distances, as compared to those in UO$_2^{2+}$"[6]. The therefore implied lower driving force to U(V) to be reduced by a second one-electron transfer renders the U(V) less susceptible to a second GSH-induced reduction. Although the already increased U(V) bond lengths foreshadow the way towards U(IV), particularly in polynuclear species dismutation is considered less effective. With regard to an interesting paper dealing with the actinyl(V) disproportionation mechanism[7] and Refs. cited therein, showing that two An(V) species form a cation–cation complex, one of which being the acceptor and the other being the donor. The initial step is a bridging of the two An(V) species by an *yl*-oxygen. Considering this, two uranyl(V) entities *within* a binuclear (polynuclear) species cannot dismutate *intra*molecularly since both the probability of

finding the necessary second U(V) within the same complex ion is quite low and neither rotation about bonds within the complex allows for such geometry. For the *yl*-oxo-bridging configuration *between* entities of *different* binuclear complex ions is impeded because of both electrostatic repulsion owing to charged ions and steric hindrance, also *inter*molecular dismutation is unlikely. Since, additionally, disproportionation involves two successive protonation reactions (thus, much more effective at low pH), the circumneutral solutions are likely to contain U(V) in sufficient amounts, also to be observed spectroscopically (*vide infra*).
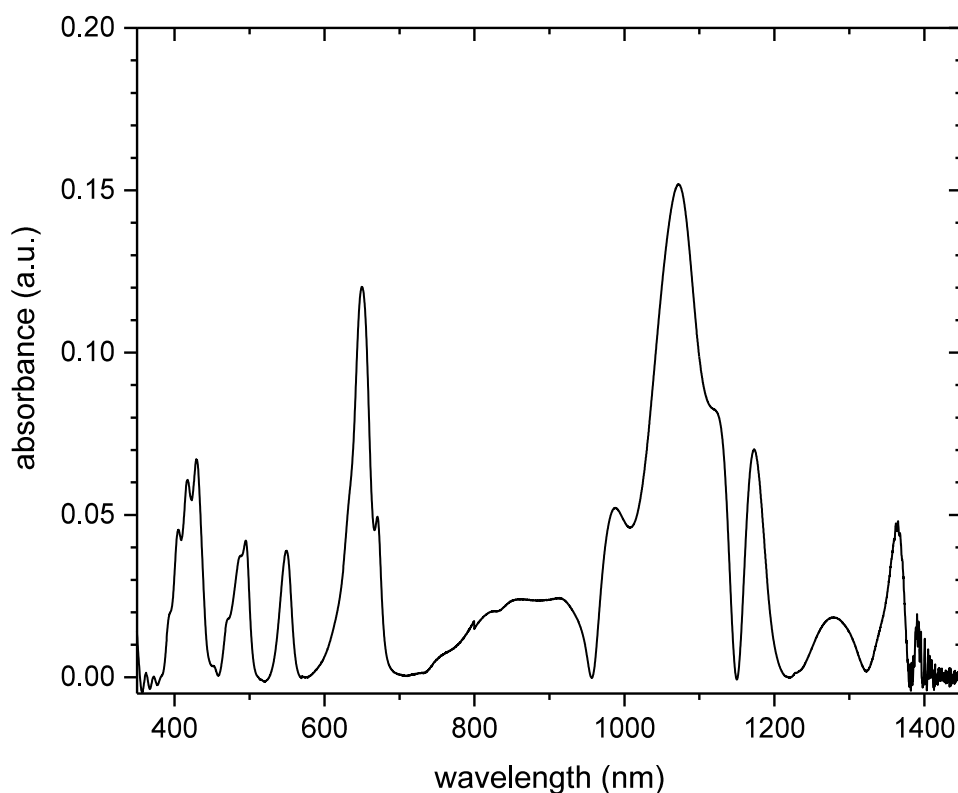
Fig. S19. UV-Vis-NIR spectrum (quartz cuvette, $d = 1$ cm) of the aged (dark brown) wet paste pellet (*cf.* Scheme S1) obtained from 10 mM GSH and 5 mM U(VI) at pH 8, after dissolution in 11 M $HClO_4$ and filtration through a 0.2 μm syringe filter, with band positions summarized in Table S4.

Table S4. UV-Vis-NIR absorption maxima according to Fig. S19.

observed (literature) absorption maxima / nm	assignment
393 (391.6)[a]	UO_2^{2+}
405.3 (402.7)[a]	UO_2^{2+}
417.5 (414.5)[a]	UO_2^{2+}
429.3 (427.0)[a] / (429.4)[b]	UO_2^{2+} / U^{4+}
470.5 (468.8)[a]	$U^{VI}O_2^{2+}$
487.3 (484.6)[a] / (485.9)[b]	UO_2^{2+} / U^{4+}
494.8 (495.3)[b]	U^{4+}
549.2 (549.5)[b]	U^{4+}
650.0 (648.5)[b]	U^{4+}
670.5 (671.6)[b]	U^{4+}
755 (738)[c] (760)[d] (770)[e]	$U^{V}O_2^{+}$
878 (880)[b]	U^{4+}
988 (940)[c] (960)[d] (990)[e,f]	$U^{V}O_2^{+}$
1073 (1069.9)[b]	U^{4+}
1124 (1132.5)[b]	U^{4+}
1172 (1140)[f]	$U^{V}O_2^{+}$
1279	$(U^{V}O_2^{+})^*$
1365	$(U^{V}O_2^{+})^*$

[a]Ref. 2; [b]Ref. 3; [c]Ref. 8; [d]Ref. 9; [e]Ref. 10; [f]Ref. 11; *assignment uncertain
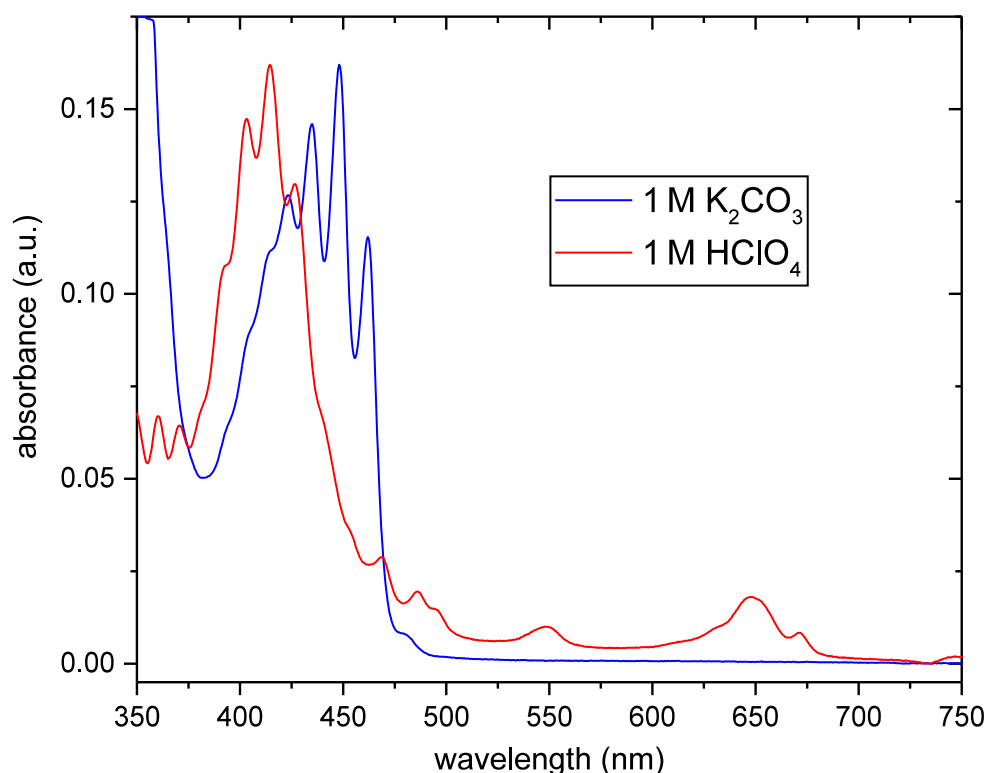
Fig. S20. UV-Vis spectrum (quartz cuvette, $d = 1$ cm) of the four weeks aged (green) wet paste pellet (*cf.* Scheme S1) obtained from 10 mM GSH and 5 mM U(VI) at pH 8 after dissolution in 1 M $HClO_4$ (red) and after extraction with 1 M K_2CO_3 (blue).

UV-Vis spectra obtained after different treatment of the aged green wet paste pellet by either 1 M $HClO_4$ or 1 M K_2CO_3 solutions revealed different absorptions (Fig. S20). Whereas dissolution in acid dissolves the material, therefore allowing for observation of U(IV) attributed absorptions ($\lambda > 500$ nm, red spectrum), the supernatant obtained after extraction with carbonate solution and subsequent centrifugation exhibits absorptions ascribed to U(VI) (hydroxo and carbonato species, blue spectrum) only. Consequently, the aged wet paste pellet contains extractable U(VI), whereas acid treatment reveals the same U(VI) fraction, and U(IV) soluble in perchloric acid, but not under alkaline conditions. As the material aged for about four weeks only, thus being bright green, substantial amounts of ternary U(VI) GSH hydroxo precursor are present in the sample. Observed U(IV) is due to formed $UO_{2(+x)}$ phases, attributed to be responsible for the colouring. Note that the apparent green colour is most likely a mixture of unreacted bright yellow ternary U(VI) and brownish U(IV)-oxide phases, the latter not dissolving in alkaline carbonate solution. Additionally, GSH was oxidised to GSSG as unambiguously proven by the COSY NMR spectrum shown in Fig. S21.
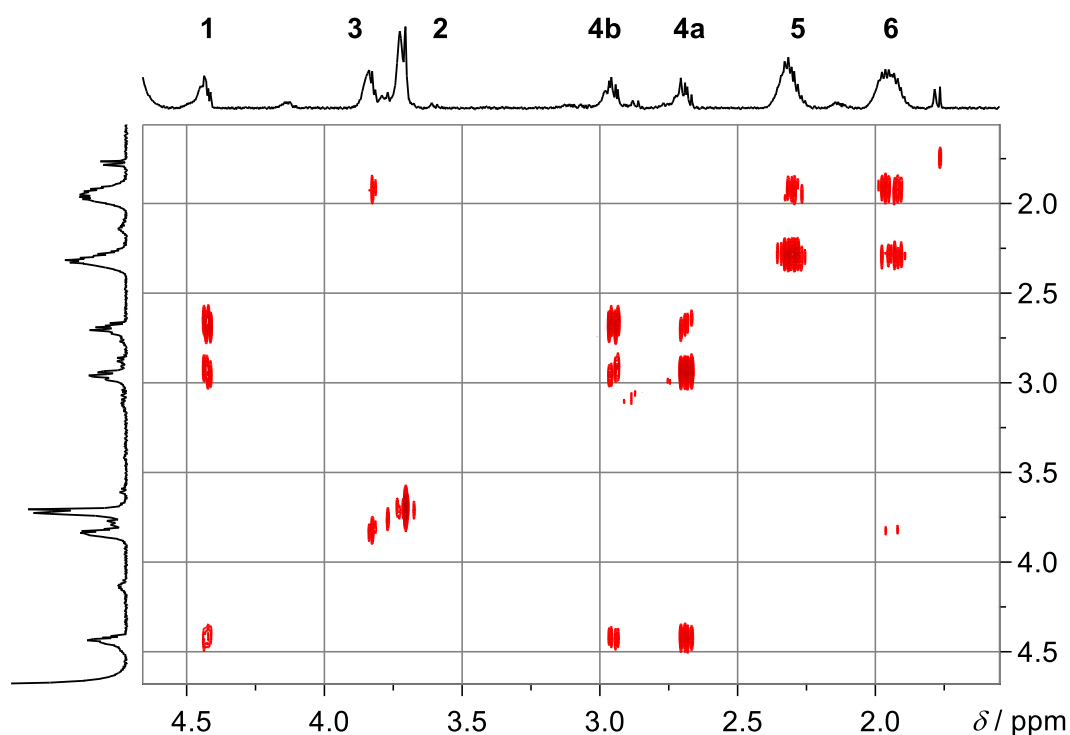
Fig. S21. H,H-COSY spectrum with ^{1}H NMR spectra (600 MHz) as external projections of the aged (olive) wet paste pellet (*cf.* Scheme S1) of the sample of initial 6.67 mM GSH and 3.33 mM U(VI) at pD 9 dissolved in 0.5 M DCl. Signals of glutathione disulphide (oxidised GSH, GSSG): **1** Cys α, **2** Gly α, **3** Glu α, **4a/b** Cys β, **5** Glu γ, **6** Glu β.

Note that the cys β protons are diastereotopic, thus showing remarkably distinct chemical shifts for GSSG unlike reduced GSH. Labelling is according to the GSH blank in Fig. S3, hence changing order of signals 2 and 3.

The broadening of the signals is ascribed to (i) the impact of the paramagnetic $U^VO_2^+$ / U^{4+} ions ($5f^1/5f^2$ electron configuration, respectively) on the bulk susceptibility rather than directly from complex formation, since the latter is unlikely in 0.5 M DCl, and (ii) high molar mass compounds: particularly at higher concentrations, U(IV) is known to form polynuclear species, clusters, and colloids. Indeed, on the one hand, high molecular mass molecules show larger rotational correlation times that cause very effective transverse relaxation (short T_2). On the other hand, once the molecules lose their solubility properties as of being not molecular dispersed any longer, the phase boundaries (between 'particle' and solvent) cause precipitous susceptibility changes and, hence, field inhomogeneities, affecting all the signals.

This interpretation is in agreement with aged (olive) wet-paste pellet material re-solubilised by ultrasonication and subjected to dynamic light scattering for particle size determination, see Fig. S22.
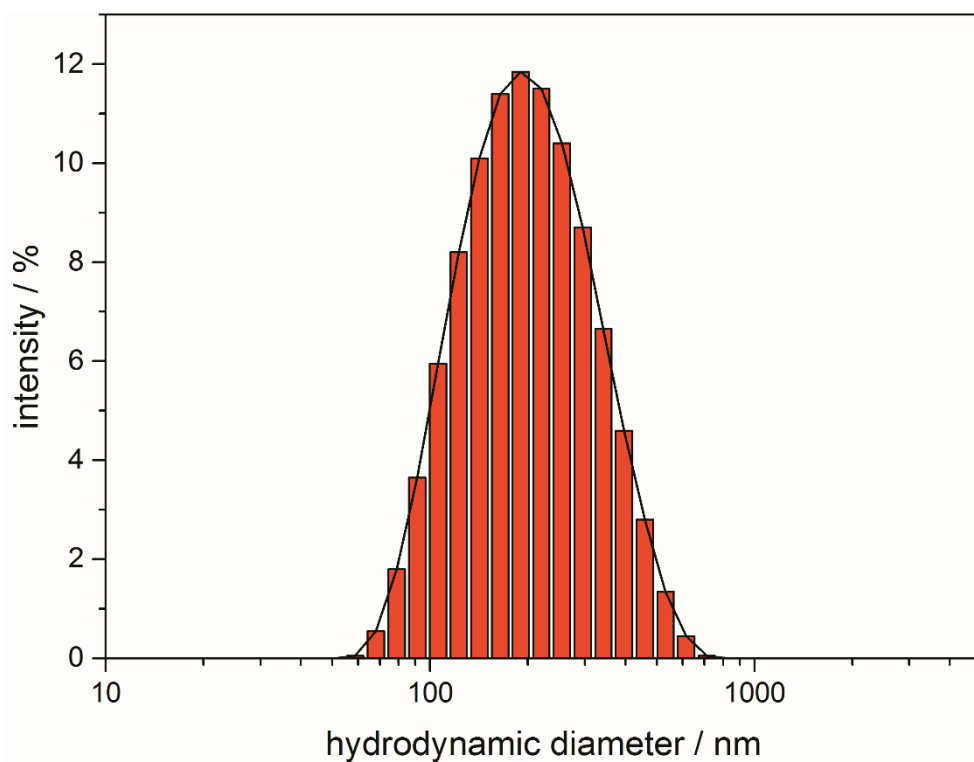
Fig. S22. Particle size distribution determined by DLS of an aliquot taken from the re-dispersed (ultrasonication) and centrifuged, aged (olive) wet paste pellet (*cf.* Scheme S1) of a sample 6.67 mM in GSH and 13.33 mM in U(VI) at pD 10.
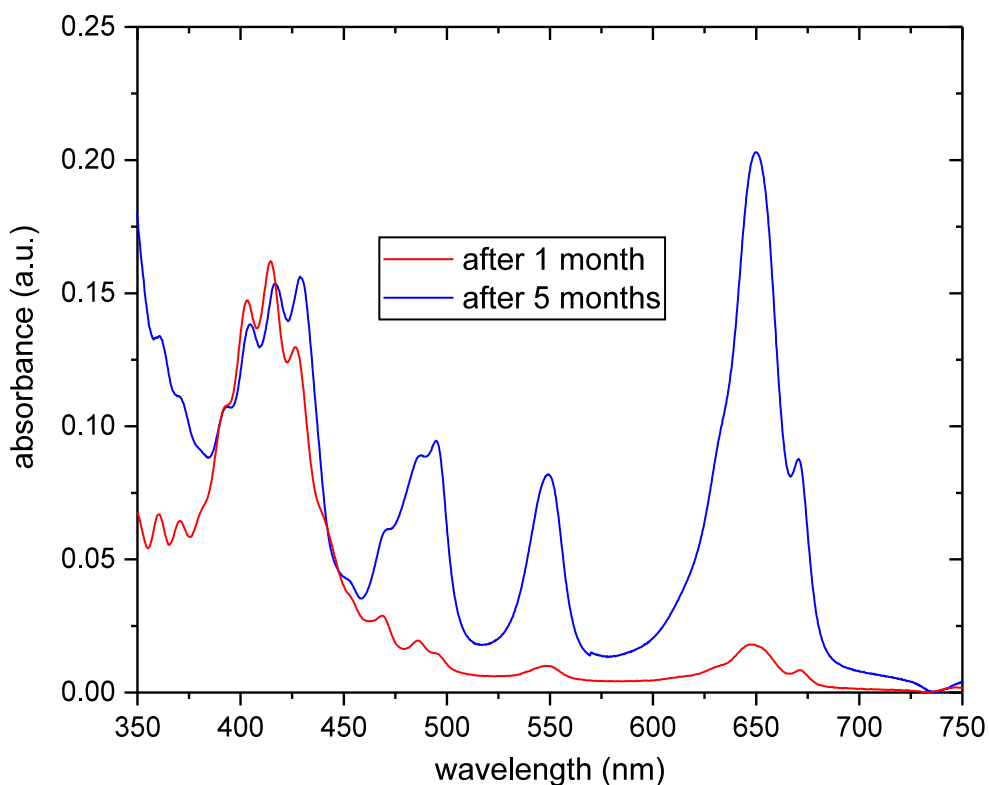
Fig. S23. UV-Vis spectra (quartz cuvette, $d = 1$ cm) of the wet paste pellet obtained from 10 mM GSH and 5 mM U(VI) at pH 8 aged for four weeks (red spectrum) and five months (blue spectrum) after dissolution in 1 M HClO$_4$, respectively.

In accordance with the observed colour changes from bright yellow *via* green and olive to brown and black (see photographs with Scheme S1), the content of reduced uranium increases as determined by U(IV) characteristic absorptions in the UV-Vis. Fig. S23 depicts spectra obtained from wet paste pellets aged for four weeks (red spectrum) and for five months (blue spectrum).

As long as the ageing pellet contains both sufficient amounts of water as the reaction medium (*i.e.*, remains wet) and free GSH as reductant, the redox reaction proceeds further. Notably, the reaction proceeds zonally, *i.e.*, from the interface between aqueous solution remaining after decantation and precipitate towards the bulk material and sample tube bottom. This is ascribed to better accessibility of the ternary U(VI) GSH hydroxo complexes to free GSH acting as reductant. Although the freshly prepared (yellow) precipitate was washed three times with 1 M NaCl solution, free GSH capable as reductant remains present in the wet paste pellet for the binding of GSH to U(VI) is labile. The latter fact is proven by solution NMR experiments (*vide infra*).
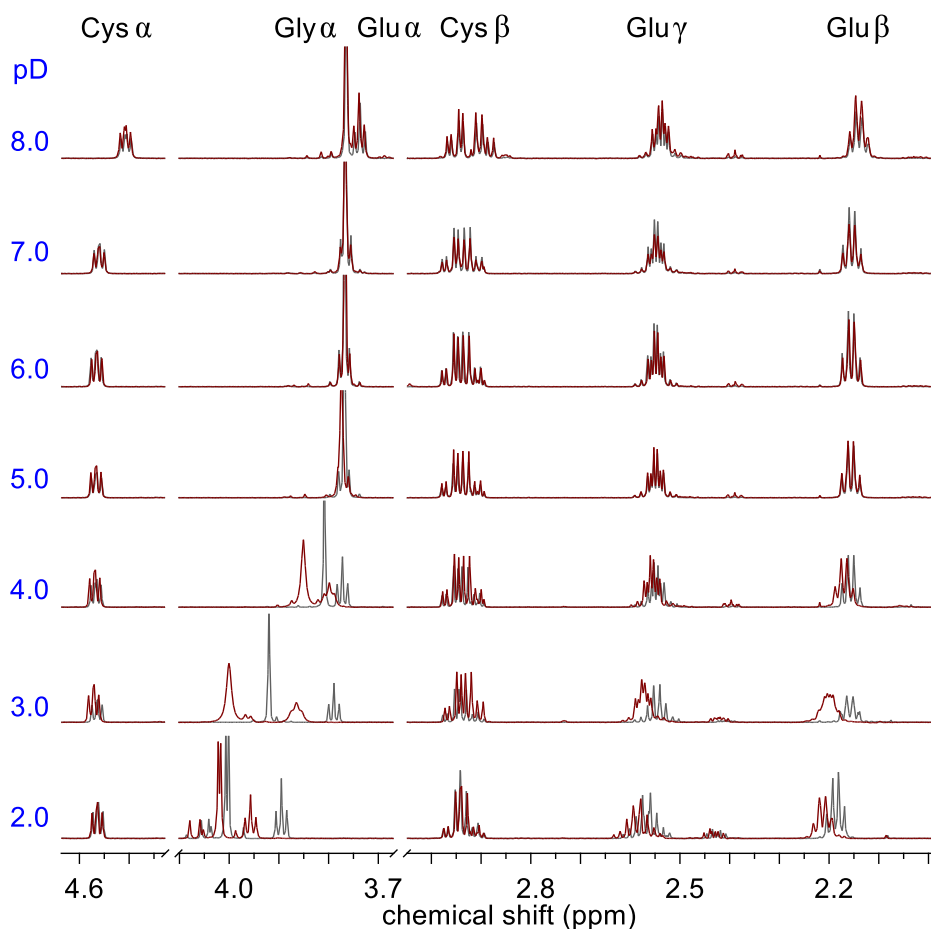
Fig. S24. ^{1}H NMR spectra of the supernatants obtained from sample series suspensions (between PS 2 and PS 4 in Scheme S1), depicted here for 6.67 mM GSH and 3.33 mM U(VI) samples with pD as indicated (corrected after centrifugation) in red, and GSH blanks in grey.

^{1}H NMR spectra representing the supernatants of freshly prepared sample series suspensions (red spectra) together with GSH blanks (grey spectra) are depicted in Fig. S24. Note that the blank signals, particularly those associated with ^{1}H close to titration sites, *i.e.*, Gly at low and Cys at high pD show shifts owing to deprotonation of Gly COOH and Cys SH, respectively. Upon interaction of GSH with U(VI), the ^{1}H signals of the different GSH sites reveal U(VI) complexation induced shifts, especially those in direct vicinity of the binding sites (carboxyl groups), that is Glu α and Gly α. For the signals of the Cys reside are virtually not affected in the presence of U(VI), complexation *via* thiol sulphur is excluded (as expected from HSAB principle).

The spectra of U(VI) and GSH solutions in principle show only one set of signals for both free and complexing GSH, *i.e.*, only averaged signals due to fast ligand exchange reaction. Thus, the apparent signal shifts the more, the higher the fraction of U(VI) bound GSH is. Consequently, the interaction (difference between grey and red spectrum at given pD) between GSH and U(VI) increases upon increasing pD, however, only up to pD ~ 3, whereas as of pD 6 virtually no difference between U(VI) containing and U(VI) free sample is observed. The latter is due to both reduced U(VI) contents upon ternary U(VI) GSH

hydroxo precipitate formation (thus decreasing the fraction of U(VI) GSH complex solution species, upon which the apparent signal is determined by free GSH fraction) and increasing competition between GSH complexation and hydrolysis (with concomitant formation of polynuclear species). Therefore, the supernatants (subsequently allowed to age) contain both U(VI) unbound GSH able to act as reductant and (polynuclear) U(VI) hydroxo species as corresponding oxidants.

A control sample kept dark the entire preparation and examination process, *i.e.* right from the mixture of GSH and U(VI), pH adjustment, ageing, and occasional analyses, showed no differences in its reaction and, thus, spectroscopic behaviour, as compared to samples handled at lab-light conditions.

REFERENCES

1. K. Müller, V. Brendler and H. Foerstendorf, *Inorg. Chem.*, 2008, **47**, 10127-10134.
2. J. T. Bell and R. E. Biggers, *J. Mol. Spectrosc.*, 1967, **22**, 262-271.
3. D. Cohen and W. T. Carnall, *J. Phys. Chem.*, 1960, **64**, 1933-1936.
4. F. Q. Schäfer and G. R. Buettner, *Free Radical Biol. Med.*, 2001, **30**, 1191-1212.
5. O. Lampela, A. H. Juffer and A. Rauk, *J. Phys. Chem. A*, 2003, **107**, 9208-9220.
6. V. Vallet, T. Privalov, U. Wahlgren and I. Grenthe, *J. Am. Chem. Soc.*, 2004, **126**, 7766-7767.
7. H. Steele and R. J. Taylor, *Inorg. Chem.*, 2007, **46**, 6311-6318.
8. J. T. Bell, H. A. Friedman and M. R. Billings, *J. Inorg. Nucl. Chem.*, 1974, **36**, 2563-2567.
9. D. Cohen, *J. Inorg. Nucl. Chem.*, 1970, **32**, 3525-3530.
10. C. Miyake, Y. Yamana, S. Imoto and H. Ohya-Nishiguchi, *Inorg. Chim. Acta*, 1984, **95**, 17-21.
11. K. Mizuoka, S. Tsushima, M. Hasegawa, T. Hoshi and Y. Ikeda, *Inorg. Chem.*, 2005, **44**, 6211-6218.